J Mater Sci: Mater Electron (2024) 35:941

Production and applications of lead (II) oxide/poly(aniline-co-thiophene) composite materials for enhanced supercapacitor performance

Ayşe V. Hacinecipoğlu[1], Selen Efeoğlu[1], Burak Kir[1], Berk Balik[1], and Metin Gencten[1,*]

[1] *Department of Metallurgy and Materials Engineering, Faculty of Chemical and Metallurgical Engineering, Yildiz Technical University, 34220 Istanbul, Turkey*

Received: 18 January 2024
Accepted: 2 May 2024

ABSTRACT

In this work, a novel approach was employed to prepare and utilize lead (II) oxide and poly(aniline-co-thiophene) (PANI-co-PTh) composite materials as electrode materials for supercapacitors, marking the first instance of such utilization in the literature. PANI-co-PTh was synthesized in bulk through chemical polymerization, and the conducting polymers underwent comprehensive spectroscopic, physical, and microscopic characterization. Subsequently, the material, incorporating lead (II) oxide (PbO) as a composite, was employed as electrode materials in asymmetric-type supercapacitors. The main results indicate a clear relationship between the surface area of conducting polymers and their specific capacitance. Notably, PANI-co-PTh-6, possessing the highest surface area, demonstrated the highest specific capacitance. Particle size distribution and specific surface area for PANI-co-PTh-6 were determined as 130 μm and 64.76 m^2g^{-1}, respectively. The PbO@PANI-co-PTh-3 configuration exhibited the highest specific capacitance, reaching 294 Fg^{-1} at a 10 mVs^{-1} scan rate. Remarkably, during long-cycle experiments, this system demonstrated a capacity retention of 70.69% after 1000 cycles. The inaugural application of the PbO@PANI-co-PTh-3 supercapacitor showcased notable capacitance values, establishing a substantial foundation for future research endeavors in this field.

1 Introduction

The unwavering pursuit of sustainable and efficient energy storage solutions stems from the growing requirements of a society advancing technologically and the pressing imperative to transition away from reliance on fossil fuels [1–3]. Energy storage assumes a crucial function in harmonizing energy production and consumption, especially vital for the seamless integration of intermittent renewable energy sources such as solar and wind power. This guarantees a steady and stable power supply even in periods without active generation [4–8]. The primary mechanisms for resilient and secure energy storage, vital for achieving sustainability, encompass batteries and capacitors [9]. Batteries, whether rechargeable or non-rechargeable,

Address correspondence to E-mail: mgencten27@gmail.com

https://doi.org/10.1007/s10854-024-12706-1
Published online: 11 May 2024

serve as devices that store chemical energy and transform it into electrical energy upon demand [10, 11]. In the realm of energy storage, supercapacitors, alternatively referred to as electrochemical capacitors or ultra-capacitors, emerge as a promising technology. Renowned for their elevated power density, rapid charge–discharge capabilities, and remarkable cycle life, supercapacitors signify a notable leap forward compared to conventional battery technology [5, 10, 12–14].

The advancement of sophisticated electrode materials plays a central role in unlocking the complete potential of supercapacitors. Researchers are progressively directing their efforts towards investigating innovative composite materials that amalgamate advantageous properties from diverse substances, aiming to enhance electrochemical performance [15–24]. While materials such as graphene, graphene hydrogel, activated carbon, metal oxides, and carbon nanotubes have been scrutinized, they frequently encounter challenges, especially in large-scale production, attributed to elevated costs [18, 22, 24, 25]. Conducting polymers have attracted considerable attention as alternative electrode materials for supercapacitors owing to their exceptional conductivity, impressive processability, and electrochemical stability [16, 24, 26]. However, despite these advantages, conducting polymers (CPs) are not exempt from drawbacks. A significant limitation lies in their low stability during repeated cycling, potentially causing performance degradation. Another challenge that necessitates attention is their susceptibility to mechanical instability under stress, leading to issues such as cracking and delamination [18, 27, 28].

Researchers are placing growing emphasis on enhancing both the mechanical and electrochemical stability of electrode materials [29]. This endeavor has prompted the investigation of hybrid materials, incorporating conducting polymers with additives like metal oxides or carbon nanotubes [24, 30–33]. These hybrid combinations exhibit improved pseudocapacitive behavior, a crucial factor for achieving high-performance supercapacitors [24, 34]. The synergy between metal oxides and conducting polymers has the potential to notably enhance specific capacitance [22, 34–37]. Through showcasing that the incorporation of metal oxides in composites yields a higher specific capacitance compared to using PTh alone, this underscores the potential of PTh doping in synergizing different materials for improved performance [21, 38–42].

The careful selection of an economical and versatile metal oxide, featuring diverse oxidation states, is crucial for optimizing composite structures [22, 24, 27, 28, 34–36]. Lead oxide emerges as a promising option due to its varied oxidation states and notable pseudocapacitive behavior when integrated with other materials [24, 35, 43–45]. Recognized for its cost-effectiveness, lead oxide enhances the durability and affordability of supercapacitors, thanks to its stability and extended cycle life [23, 44, 45]. Its capacity to operate across a wide voltage range adds versatility for various supercapacitor applications [18, 23, 39, 40, 42, 43, 45]. The composite examined in this study combines lead (II) oxide (PbO) with PANI-co-PTh, leveraging the synergistic effects of conducting polymers and lead oxide. This has the potential to yield higher energy densities, improved stability, and enhanced cycling performance compared to using pure materials [40, 43–45].

Asymmetric supercapacitors (ASCs), with their widened voltage range, provide greater energy density. Metal oxides like PbO, MnO_2, Co_3O_4, and Fe_3O_4, known for their pseudocapacitive behavior, encounter challenges such as limited ionic diffusion and poor conductivity. Integrating MnO_2 with conductive substrates aims to improve energy storage performance [46]. Various research teams have explored combining metal oxides with carbon-based materials (such as activated carbon, carbon fibers, graphene, nanotubes, and carbon spheres), conducting polymers (like polyaniline and polypyrrole), and other metal oxide materials (such as NiO, Co_3O_4 and TiO_2) to address these challenges [46–48].

Extensive research has been undertaken on conducting polymers (CPs) such as polyaniline (PANI), polypyrrole (PPy), and polythiophene (PTh) within the realms of supercapacitors, batteries, and electro-optical devices [17, 28, 34–36, 49–51]. The progression of supercapacitor technology has witnessed notable strides in the design of electrode materials, with a specific emphasis on CPs like PANI and PTh. A seminal study employing spin coating to create thin films of these polymers revealed that PANI-based supercapacitors exhibit a specific capacitance four times greater than counterparts using PTh alone [42]. This discovery underscores the potential of PANI in augmenting the efficiency of supercapacitors.

Polythiophene is esteemed for its straightforward synthesis, environmental stability, and commendable cycle durability [24, 39]. However, its drawbacks in terms of conductivity and specific capacitance can be

mitigated by copolymerizing it with PANI [39, 40, 42]. This copolymerization strategy enhances the overall performance of the electrode material. The resulting composites, achieved by combining conducting polymers with lead oxide, exhibit high conductivity, flexibility, and increased specific capacitance, rendering them well-suited for supercapacitor electrodes [29, 40, 45, 52, 53]. PTh remains a popular choice for energy storage applications owing to its straightforward synthesis and stability [54–57]. Nevertheless, it encounters constraints concerning conductivity and capacitance. To surmount these limitations, PANI can be copolymerized with polythiophene, effectively augmenting conductivity and stability, thereby proving essential for supercapacitors [20, 40, 42]. Our investigation delves into PANI-co-PTh composites, harmonizing the strengths of both polymers to yield elevated conductivity, flexibility, and enhanced capacitance. This copolymerization not only improves the electrical properties of the material but also enhances its processability and mechanical strength.

Some synthesis approaches for polyaniline, polythiophene, and their copolymers have been proposed [40, 42]. These methods involve techniques like interfacial and aqueous polymerization, necessitating prolonged reactions at specific boiling points for aniline and thiophene, intricate purification steps, and the application of high temperatures [52, 53]. Moreover, many of these procedures utilize harmful toxic chemicals, with the use of chloroform as a solvent contributing to environmental concerns due to its classification as a volatile organic compound [52, 53, 58]. In this study, we employed simple, environmentally friendly, cost-effective, and chemical methods that eliminate the need for harmful chemical reductants. Notably, lead (II) oxide was introduced for the first time in the literature to the prepared PANI-co-PTh-based conducting polymers, facilitating the fabrication of asymmetric coin cell type supercapacitors in this work.

2 Experimental

2.1 Synthesis of PANI-co-PThs

The synthesis of PANI-co-PThs involved solutions containing 1.0 M sulfuric acid (H_2SO_4, Merck, > 98%) and varying concentrations of monomers at 60 °C. Specifically, 0.5 M aniline (> 99.5%, Sigma-Aldrich) and thiophene (> 99, Merck) were combined in volume ratios of 1:1, 2:1, 3:1, and 4:1, as outlined in Table 1, to produce copolymers. While the oxidant used in the preparation of CPs was $FeCl_3$ (ferric chloride, > 97%, Sigma-Aldrich), sulfuric acid (98%, Sigma-Aldrich) was used as the acid. Subsequently, the copolymer synthesis continued with a fixed monomer concentration (0.375 M aniline and 0.125 M thiophene) while altering sulfuric acid concentrations, as detailed in Table 1. The entire synthesis procedure lasted 3 h and occurred in a 250-mL flask under reflux and atmospheric conditions [51, 59]. Following synthesis, the resulting powders underwent filtration, washing with distilled water, and drying in an oven at 60 °C for 6 h. These dried powders served as electrode materials for supercapacitors.

2.2 Characterization of CPs

Various techniques were employed to assess the spectroscopic, microscopic, thermal, and physical characteristics of CPs. Scanning electron microscopy (SEM) analyses were conducted at 30,000×magnification using a Zeiss EVO® LS 10 after applying a 30s gold coating at 20 mA. To determine the chemical structure of the materials, SEM–EDX analyses were carried out. The surface area of the prepared CPs was assessed through Brunauer-Emmet-Teller (BET) analysis, utilizing Quantachrome Corporation's Autosorb-6 instrument. Fourier Transform Infrared Spectroscopy (FT-IR) analyses were performed using Perkin Elmer Spectrum 100 equipment. Particle size distribution of the CPs was determined with a Malvern Hydro 2000 MU model mastersizer. Thermal analyses were undertaken using the SII6000 Exstar TG/DTA 6300 model TG/DTA device, with a 5 °C increment per minute within the temperature range of 25 to 1000 °C. The

Table 1 Lists the given names and the conditions under which CPs were prepared at 60 °C

Molar ratio of PANI/PTh	Concentration of H_2SO_4/M	Concentration of $FeCl_3$ /M	Code of CPs
3: 1	1.0	0.1	PANI-co-PTh-1
1: 1	1.0	0.1	PANI-co-PTh-2
2: 1	1.0	0.1	PANI-co-PTh-3
4: 1	1.0	0.1	PANI-co-PTh-4
3: 1	0.1	0.1	PANI-co-PTh-5
3: 1	0.5	0.1	PANI-co-PTh-6
3: 1	2.0	0.1	PANI-co-PTh-7

electrochemical behaviors of the composite materials were investigated using a Gamry Interface 1010B model potentiostat/galvanostat within the framework of the employed electrochemical measurement system.

2.3 Coin-cell type preparation of and electrochemical characterization with CPs

Table 2 illustrates the composition of a mixture containing 3 mL N-methyl pyrrolidone (NMP), 0.04 g carbon black, 0.04 g PVDF (polyvinylidene fluoride), and three different ratios of CPs and lead (II) oxide. Each supercapacitor employed the optimal polymer blend, designated as PANI-co-PTh-6. To create efficient coin cell type supercapacitor electrodes, three distinct active material mixtures, each totaling 0.4 g (see Table 1), were prepared. The resulting mixture underwent thorough blending in an ultrasonic bath for 30 min. Using a doctor blade, a 200-micron thick film was formed on aluminum foil [51, 59, 60]. Subsequently, the film was dried in an oven at 90 °C for a day to eliminate the solvent [51, 59, 61]. Circular electrodes with a 16 mm diameter were then cut from the film using a cutting machine. The fabrication process for the counter electrode mirrored that of the working electrode, with the exception that nano graphite powder, specifically sized between 15 to 20 nm, was used instead of CP [59]. An asymmetrical CR2032 type supercapacitor was assembled with a 1.0 M sulfuric acid electrolyte, and the electrodes were separated by a 16 mm diameter porous membrane [60, 61]. To prepare the coin cell for electrochemical testing, it was sealed under pressure to eliminate any open areas [62]. The capacitive performance of these coin cell type supercapacitors was assessed through cyclic voltammetry and charge–discharge tests.

Table 2 PbO-based CPs prepared for use in coin-cell type asymmetric supercapacitors and given name

Code of PbO-based CPs	PbO (%)	PANI-co-PTh-6 CP (%)	PVDF (%)	Carbon black (%)
PbO@PANI-co-PTh-1	40	40	10	10
PbO@PANI-co-PTh-2	50	30	10	10
PbO@PANI-co-PTh-3	60	20	10	10

3 Results and discussions

3.1 Characterization of PANI-co-PTh by BET and FT-IR analysis

Conducting polymers (CPs) were synthesized chemically using various monomer ratios in a solution of 1.0 M sulfuric acid and 0.1 M $FeCl_3$. Table 3 provides details on the acronyms and synthesis conditions for the CPs utilized in the study, along with the Brunauer–Emmett–Teller (BET) surface area analysis of the synthesized nanomaterials. The nitrogen adsorption properties of PANI-co-PTh-1 in the solid state at 77.3 K, including BET surface area analysis and total pore volume, are outlined. The BET analysis indicated that the sample with the maximum surface area exhibited the highest specific capacitance. Consequently, in the subsequent step, the PANI-co-PTh-1 experiment with a maximum surface area of 41.393 m^2g^{-1} was selected to conduct experiments determining the optimum acidic concentration. The BET analysis consistently revealed that larger surface areas in electrode materials contribute to enhanced capacitance in supercapacitors, aligning with established

Table 3 Surface areas of the produced copolymers as a result of BET analysis under different monomer and acid concentrations

Molar ratio of PANI/PTh	Concentration of H_2SO_4/M	Concentration of $FeCl_3$ /M	Surface area (m^2 g^{-1}) (BET)	Code of CPs
3:1	1.0	0.1	41.39	PANI-co-PTh-1
1:1	1.0	0.1	38.92	PANI-co-PTh-2
2:1	1.0	0.1	14.52	PANI-co-PTh-3
4:1	1.0	0.1	26.49	PANI-co-PTh-4
3:1	0.1	0.1	58.26	PANI-co-PTh-5
3:1	0.5	0.1	64.97	PANI-co-PTh-6
3:1	2.0	0.1	62.33	PANI-co-PTh-7

knowledge in this field [12, 35, 42, 50, 63]. The samples were analyzed using the BET device, and the results showed that the PANI-co-PTh-6, utilizing 0.5 M sulfuric acid, achieved the highest surface area recorded at 64.97 m^2g^{-1}. Additionally, Li and Wu et al. investigated the influence of varying shapes of different metal oxides and metal sulfides on capacitance performance [64–66]. They synthesized these electrodes while controlling the shape of the materials, resulting in structures with well-defined features and optimal pore distribution. Such structures provide larger effective specific surface areas, offering abundant electroactive sites and facilitating ion transport, thereby demonstrating ultra-high electrochemical performance [64–67].

FT-IR analysis was conducted to chemically characterize the conducting polymers. The FT-IR spectra of PANI-co-PTh-6, representing the optimized CP blend, are illustrated in Fig. 1. The N–H bonds' peak range, attributed to the structure of polyaniline, is estimated between 3100 and 3450 cm^{-1} (Fig. 1) [40, 68]. The FT-IR spectrum of PANI-co-PTh-6 reveals peaks at 1535 and 1487 cm^{-1}, denoting the quinoid ring and benzenoid ring C=C stretching modes. Peaks at 1418 cm^{-1} emerge due to C–C stretching vibrations in the aromatic ring [33, 40]. The C-N stretch specific to secondary amines in both PANI and PANI-co-PTh appears at 1250–1320 cm^{-1}. Additionally, the spectra of doped PTh exhibit primary peaks at 701 cm^{-1}, primarily attributed to C–S stretching. The peaks at 3146, 1401, and 1687 cm^{-1} are linked to the C–C, C–H, and C=C stretching vibrations of the aromatic ring, respectively [69, 70].

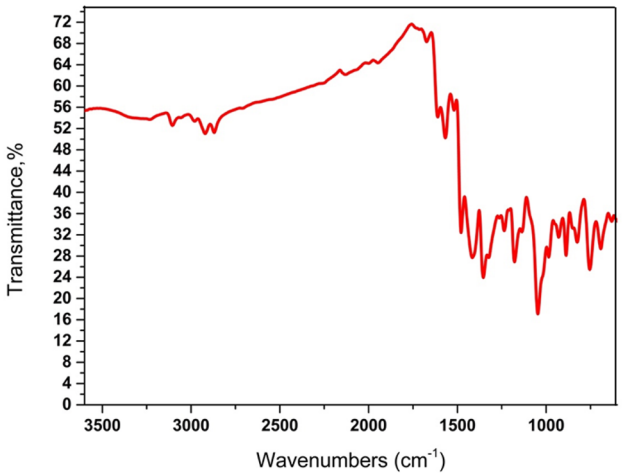

Fig. 1 FT-IR spectrum of PANI-co-PTh-6

3.2 Characterization of PANI-co-PTh by SEM analysis

SEM analyses were conducted to assess the morphological characteristics of conducting polymers. Figures 2a–d depict the SEM images of PANI-co-PTh-2, PANI-co-PTh-3, PANI-co-PTh-1, and PANI-co-PTh-4, respectively. Polyaniline typically exhibits a more

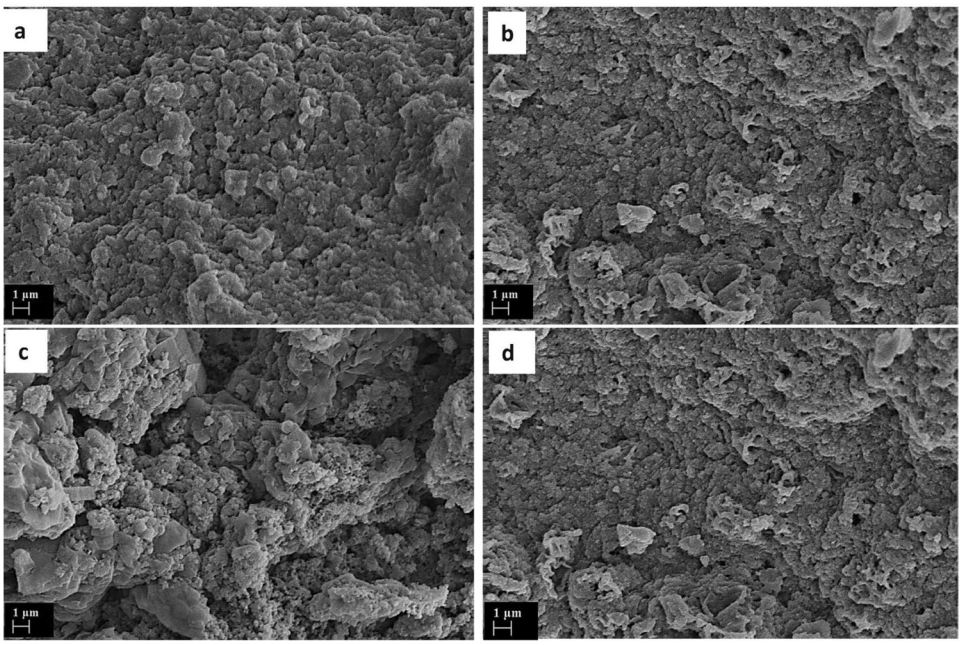

Fig. 2 10,000× SEM pictures of **a** PANI-co-PTh-2, **b** PANI-co-PTh-3, **c** PANI-co-PTh-1 and **d** PANI-co-PTh-4

organized, layered structure due to its cyclic aromatic rings and amine groups, in contrast to polythiophene, which features a distinct structure composed of thiophene rings [33, 71]. The multilayer structure of PANI-co-PTh nanocomposites is visibly porous in Figs. 2 and 3. The addition of PbO to PTh enhances its capacitive properties due to the porous nature that facilitates charge storage. The SEM images reveal the spherical structure of PTh nanocomposites and the porous structure of PANI nanocomposites, influencing homogeneity, size distribution, morphology, and polymer synthesis. The SEM image of a copolymer produced through chemical synthesis with polythiophene-polyaniline copolymer is influenced by various factors, including synthesis conditions and polymer ratios. Copolymerization results in a more homogeneous material with a distinct morphology compared to pure PTh or PANI. The unique surface structure or pattern feature of the copolymer is evident in the SEM images (Figs. 2, 3). Depending on the specific synthesis conditions outlined in Table 1, aggregated structures or particles were observed on the copolymer's surface. The presence of $FeCl_3$ may have contributed to the formation of nanoparticles or other structures, as observed in the SEM image in Fig. 2 [33, 58, 70]. As a result of BET analysis, the PANI-co-PTh-1 coded powder sample (41.39 m^2/g), as shown in Fig. 2c, exhibited the highest surface area and formed a notably porous structure compared to the other samples [31, 40]. This porosity is attributed to the extensive surface area, and the bulk structure observed on the surface aligns with SEM images encountered in existing literature studies, serving as evidence of successful copolymer synthesis through low-cost, simple, and effective chemical polymerization.

The surface morphologies resulting from the optimization of sulfuric acid concentration are depicted in Fig. 3. Based on the BET analysis outcomes, the highest surface area, reaching 64.97 m^2g^{-1}, was achieved on the surfaces of conducting polymers prepared in a solution containing 0.5 M sulfuric acid (Fig. 3b). However, surface roughness was observed on the spheres of PANI-co-PTh prepared in sulfuric acid. In summary, the SEM images for PANI-co-PTh-1 and PANI-co-PTh-6 substantiate the successful production of CPs in accordance with the literature. The chemical compositions of CPs were further explored through Energy Dispersive X-ray Spectroscopy (EDS) analyses (Fig. 4). The presence of nitrogen, an expected element for polyaniline, indicates the existence of aniline units. Additionally, the characteristic sulfur atom at the center signifies the presence of thiophene rings.

The significant enhancement in surface area observed in PANI-co-PTh-6 compared to other synthesized composite samples can be attributed to the systematic variation of monomer ratios and sulfuric

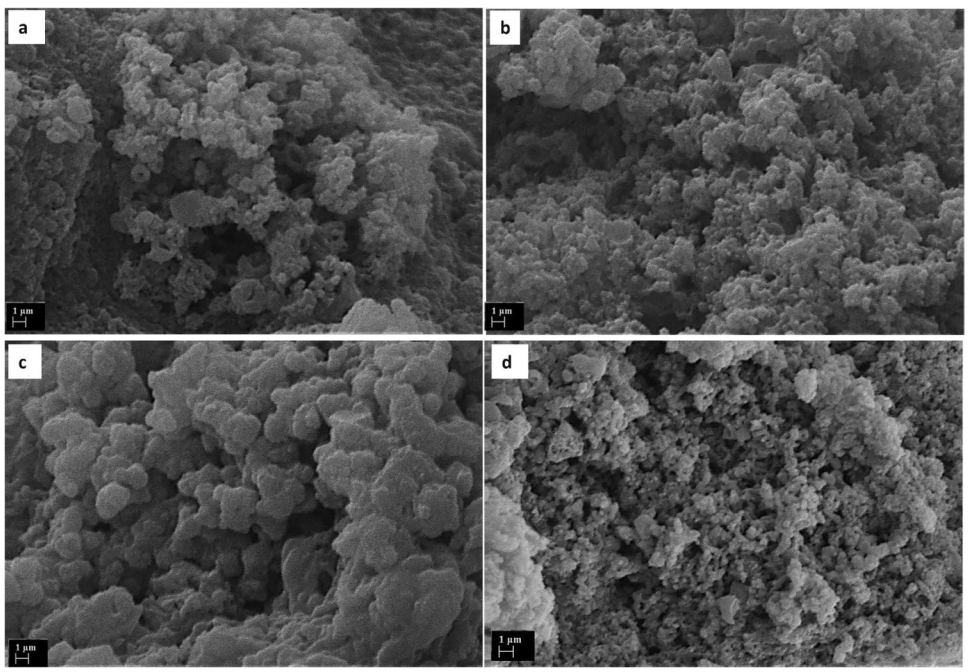

Fig. 3 40,000× SEM pictures of **a** PANI-co-PTh-5, **b** PANI-co-PTh-6, **c** PANI-co-PTh-1 and **d** PANI-co-PTh-7

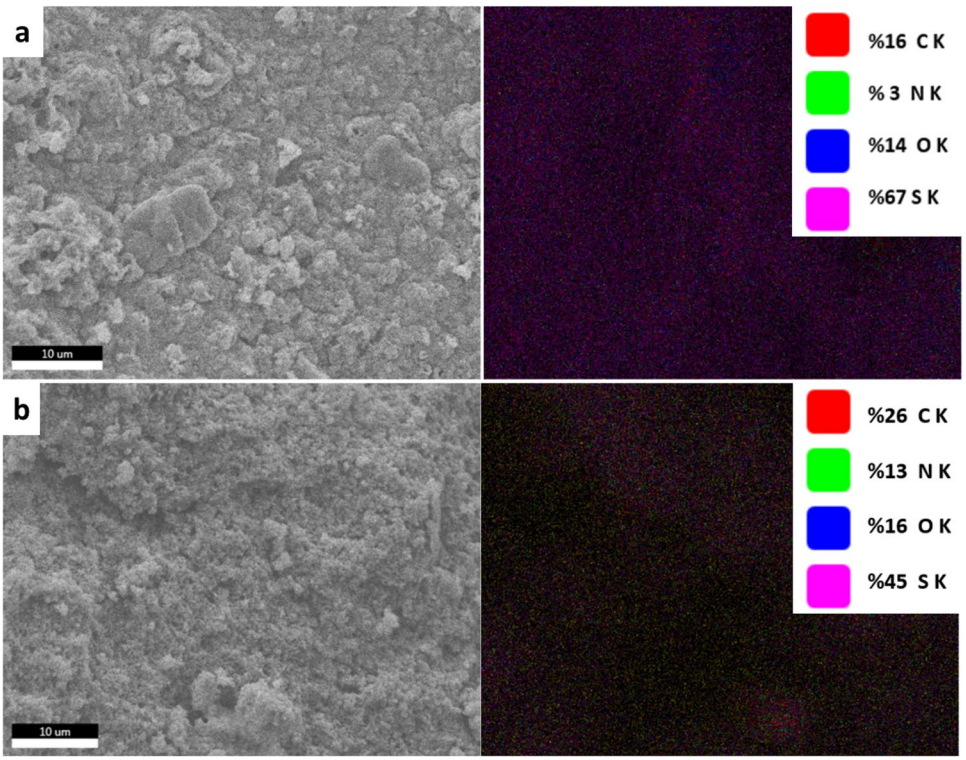

Fig. 4 EDS mapping of **a** PANI-co-PTh-1 and **b** PANI-co-PTh-6

acid concentrations during the synthesis process. This optimization strategy enabled precise control over the structural characteristics of the CPs, facilitating the formation of porous networks conducive to enhanced electrochemical activity and specific capacitance in supercapacitor applications.

3.3 Thermal and physical characterizations of PANI-co-PThs

The thermal behavior of PANI-co-PTh-6 conducting polymer (CP) was investigated through TG/DTA analysis. The thermograms displayed in Fig. 5 reveal that the thermal degradation of PANI-co-PTh-6 occurs in multiple stages [33].

In the first stage, it experiences a mass loss of 11.7% between 100 and 320 °C, attributed to the removal of water from the structure and the decomposition of prepolymers. Subsequently, in the second stage, a mass loss of 65.7% is observed between 150 and 400 °C. Peaks at 130 °C and 330 °C signify the thermal degradation of large polymer chains, involving the loss of energy and mass. Mass losses beyond 250 °C are indicative of polymer degradation. Furthermore, copolymers exhibit distinct thermal behaviors from both homopolymers and each other [40]. PANI undergoes a two-step degradation, while PTh undergoes a single-step degradation [40]. These differing thermal behaviors suggest that the polymers synthesized in a solution containing aniline and thiophene monomers form a PANI-co-PTh copolymer [72]. Additionally, uniquely designed hemoglobin-like composites comprising CoP nanoparticles coated with N,P-doped carbon shell (CoP@PNC) were prepared via a supramolecular self-assembly method,, with the TG curve reaching a steady state at 800 °C. Furthermore, a separate study involved the synthesis of 3D porous N-doped carbon decorated with MoO_2 nanoparticles [73, 74].

Figure 6 illustrates the particle size distribution plot for PANI-co-PTh-6 materials, revealing an average particle size of 130 µm. Additionally, according to BET analysis, PANI-co-PTh-6 exhibits the highest surface area and an average particle size of 64.9 m^2g^{-1} and 130 µm, respectively.

3.4 Supercapacitor application of PbO@PANI-co-PThs

Capacitive behavior of asymmetric supercapacitors composed of PbO@PANI-co-PTh-1, PbO@PANI-co-PTh-2, and PbO@PANI-co-PTh-3 was

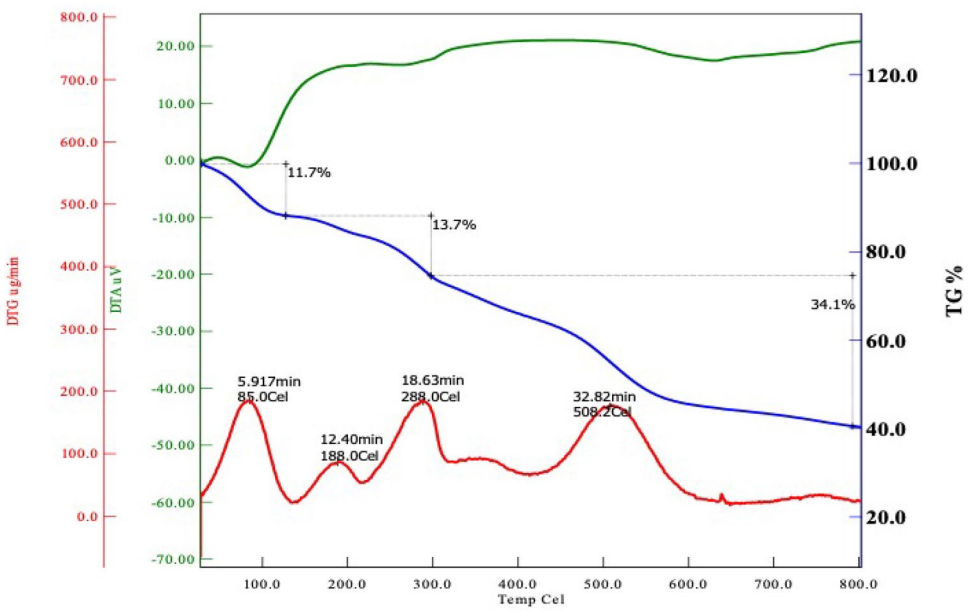

Fig. 5 TG/DTA thermogram of PANI-co-PTh-6

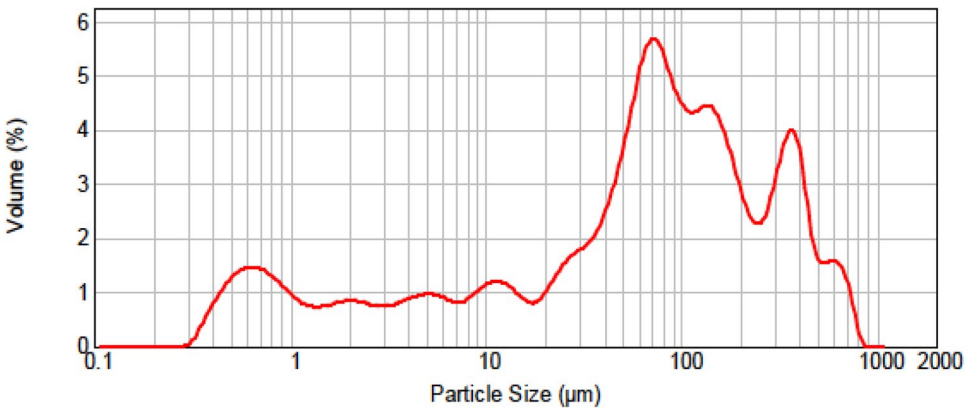

Fig. 6 Particle size distribution of PANI-co-PTh-6

investigated by cyclic voltammetric analyses and cyclic charge–discharge tests. The cyclic voltammograms provide insights into the materials' capacitance through the analysis of currents and rectangular patterns. Specific capacitances of the asymmetric supercapacitors were calculated using Eq. 1, where the variables C, I, Δt, A, and ΔV represent specific capacitance, charge/discharge current, time spent charging/discharging, electrode surface area, and voltage differential for charging/discharging, respectively [75–77].

$$C = \frac{I.\Delta t}{\Delta V.\,A} \quad (1)$$

Cyclic voltammetric analyses were conducted to assess the electrochemical behaviors of supercapacitors incorporating PbO and PANI-co-PTh-based conducting polymers (CPs) across various potential ranges. Figure 7 displays the cyclic voltammograms of PbO@PANI-co-PTh-3, representing an asymmetric supercapacitor. Based on anodic and cathodic peak area and peak currents, the highest capacitive behavior was observed within the potential range of − 0.8 V to + 1.5 V. The redox peaks originating from PbO and PANI-co-PTh significantly contributed to the pseudocapacitive behavior of the CPs. Notably, no gas evolution was observed within this potential range. Consequently, the optimal operating potential range for the asymmetric supercapacitor, incorporating PbO and PANI-co-PTh with a 1.0 M sulfuric acid electrolyte, was determined as − 0.8 V to + 1.5 V. Subsequently, cyclic voltammetric analysis was conducted at various scan rates to calculate the specific capacitances of PbO@PANI-co-PTh-1, PbO@PANI-co-PTh-2, and PbO@PANI-co-PTh-3 in 1.0 M sulfuric

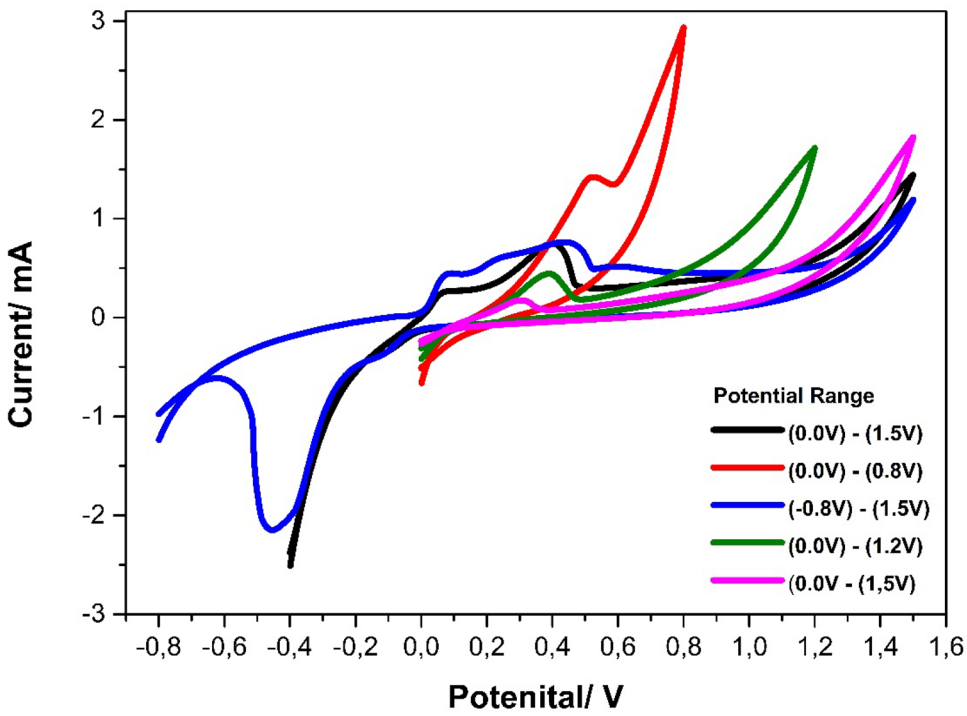

Fig. 7 Voltamograms of PbO@PANI-co-PTh-3 asymmetric-type supercapacitors at different potential ranges in 1.0 M sulfuric acid

acid, as depicted in Figs. 8a–c, respectively. The gradual increase in peak currents with rising scan rates suggests that diffusion primarily contributes to mass transfer to the electrode surfaces. All prepared nanocomposites exhibited a distinct peak during positive or negative scans in the cyclic voltammograms. The observed semi-rectangular shapes for cathodic and anodic peaks validate the stable electrochemical properties of the nanocomposites, indicating exceptional capacitive performance at 10 mV/s. PbO@PANI-co-PTh-3 nanocomposites displayed better electrochemical performance compared to other nanocomposites and pure PTh due to their wider curve area and high specific capacitance. The redox reaction is more pronounced and distinct for PbO@PANI-co-PTh-3 compared to PbO@PANI-co-PTh-1 and PbO@PANI-co-PTh-2, attributed to the presence of more PbO nanoparticles on the matrix. Hence, the shape of this curve precisely resembles a semi-rectangular shape with a broad curved area [78]. To better elucidate the reaction kinetics and mechanism contribution underlying the integrated PbO@PANI-co-PThs hybrid system, cyclic voltammetry (CV) measurements were conducted for hybrid systems PbO@PANI-co-PTh-1, PbO@PANI-co-PTh-2, and PbO@PANI-co-PTh-3 at various low scan rates ranging from 10 to 500 mV/s. Detailed CVs are illustrated in Fig. 8a–c. It is evident from the CV curves of the hybrid system that they exhibit two distinct oxidation peaks and one reduction peak. Furthermore, the oxidation and reduction peaks gradually broaden, and the peak current response increases with the increasing scan rate, while the configuration of the CV curves remains consistent at all scan rates [79]. It is observed that PANI exhibits an oxidation peak potential of approximately + 0.2 V versus Ag/AgCl, while thiophene demonstrates an oxidation peak potential of approximately + 1.2 V versus Ag/AgCl [79]. The oxidation peak at 1.2 V and the reduction peak at − 0.2 V observed for the PbO electrode are consistent with phase transitions among PbO species as reported in previous studies. These findings corroborate the expected behavior of lead(II) oxide (PbO) in electrochemical systems, where it undergoes reversible oxidation–reduction processes, contributing to the overall electrochemical performance of the hybrid system. The synergistic effect among PbO nanoparticles in this nanocomposite may enhance pseudocapacitive performance. The increased surface area of PbO nanoparticles surrounded by PANI-co-PTh supports an improved interaction mechanism between nanocomposites and the electrolyte for electrochemical energy conversion [45, 78–80]. Additionally, electron transfer in metal oxide nanoparticles is enhanced by intercalation within the PANI-co-PTh matrix, leading to good charge storage capacity and excellent kinetic response for PANI-co-PTh and PbO nanocomposites.

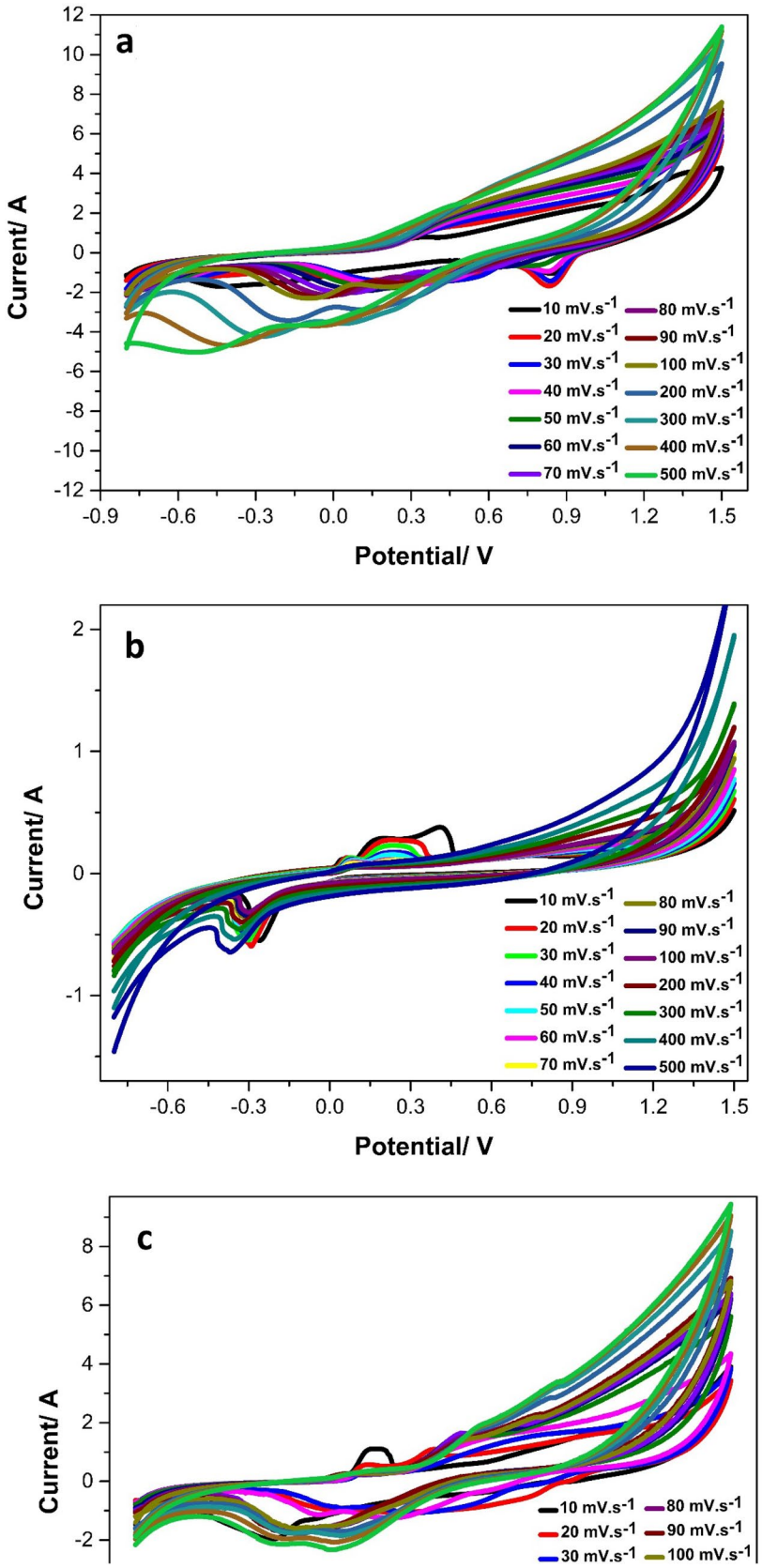

Fig. 8 Cyclic voltammograms and different scan rates of asymmetric-type supercapacitors based on **a** PbO@PANI-co-PTh-1, **b** PbO@PANI-co-PTh-2, and **c** PbO@PANI-co-PTh-3, respectively, in 1.0 M sulfuric acid

In PbO@PANI-co-PTh-3 nanocomposites for energy storage applications, the synergistic effect between PbO nanoparticles and PANI (polyaniline) and PTh (polythiophene) can be understood through a deeper discussion of theoretical context and underlying mechanisms. PbO nanoparticles possess intrinsic conductivity due to their electronic structures [78, 80]. Concurrently, PTh, being a conjugated polymer, also exhibits high electrical conductivity. The interaction between PbO nanoparticles and PANI-co-PTh in the nanocomposite facilitates pathways for electron transport, thereby facilitating rapid charge/discharge processes in energy storage devices. This conductivity enhancement is crucial for improving the overall efficiency and performance of the electrode. PbO nanoparticles offer a wide surface area with ample active regions for electrochemical reactions. PANI-co-PTh serves as a stabilizing matrix, aiding in the dispersion and immobilization of nanoparticles within the composite. The synergy between PbO nanoparticles and PANI-co-PTh enhances accessibility and utilization of active regions, leading to increased electrochemical activity and energy storage capacity. The porous structure of PbO nanoparticles, combined with interconnected PANI-co-PTh network, facilitates ion diffusion within the electrode. This synergistic effect enhances the diffusion of ions to and from active regions, reduces diffusion limitations, and improves the charge/discharge kinetics of the electrode. PANI-co-PTh provides mechanical support and flexibility to the nanocomposite electrode, preventing agglomeration and structural degradation of PbO nanoparticles during cycling. PbO nanoparticles, in turn, enhance the mechanical strength of PANI-co-PTh by preserving the structural integrity of the electrode under repeated charge/discharge cycles. The synergistic interaction between PbO nanoparticles and PTh ensures long-term stability and durability of the electrode, crucial for reliable performance in energy storage applications. The combination of PbO nanoparticles and PTh may lead to synergistic redox reactions, where both components interact to enhance the overall charge storage capabilities of redox-active species. This synergy in redox chemistry could further enhance the energy storage performance of the nanocomposite electrode. Therefore, the synergistic effect between PbO nanoparticles and PANI-co-PTh in PbO@PANI-co-PTh-3 nanocomposite electrode for energy storage applications arises from complementary properties and interactions at various levels, including enhanced conductivity, increased active regions, improved ion diffusion, structural stability, and potentially synergistic redox chemistry [42, 78, 80]. At a scan rate of 10 mVs^{-1}, the specific capacitances were determined as 48.91 $F.g^{-1}$, 51.04 $F.g^{-1}$, and 294.02 $F.g^{-1}$ for PbO@PANI-co-PTh-1, PbO@PANI-co-PTh-2, and PbO@PANI-co-PTh-3, respectively (Tables 4 and 5). The higher lead (II) oxide content (60%) in PbO@PANI-co-PTh-3 contributed to its superior specific capacitance value. The coin cell with the largest area at a scan rate of 10 mVs^{-1} among PbO@PANI-co-PTh-1, PbO@PANI-co-PTh-2, and PbO@PANI-co-PTh-3 was PbO@PANI-co-PTh-3 in cyclic voltammograms given in Fig. 9, considered optimal for subsequent studies. Moreover, the specific capacitance value of PbO@PANI-co-PTh-3 surpassed that of PbO@PANI-co-PTh-1 and PbO@PANI-co-PTh-2 (Table 4). The addition of lead oxide species to polyaniline and polythiophene imparted a more capacitive behavior to the materials. Consequently, the asymmetric supercapacitor with a higher proportion of PbO materials exhibited a greater

Table 5 Specific capacitance comparison of the asymmetric-type supercapacitors consisting of PbO@PANI-co-PTh-1, PbO@PANI-co-PTh-2 and PbO@PANI-co-PTh-3, respectively

Coin cell type	V/s	ΔV	Cs (Fg^{-1})
PbO@PANI-co-PTh-1	0.010	2.3	48.9
PbO@PANI-co-PTh-2	0.010	2.3	51.0
PbO@PANI-co-PTh-3	0.010	2.3	294.0

Table 4 Specific capacitance of asymmetric-type supercapacitors consisting of PbO@PANI-co-PTh-1, PbO@PANI-co-PTh-2 and PbO@PANI-co-PTh-3 in 1.0 M sulfuric acid

Scan rate/mVs^{-1}	10	20	30	40	50	60	70	80	90	100	200	300	400	500
Material	Specific capacitance as Fg^{-1} at different scan rates													
PbO@PANI-co-PTh-1	48.9	28.5	18.5	14.9	11.9	10.4	9.3	8.4	7.6	6.9	4.4	3.3	2.5	2.0
PbO@PANI-co-PTh-2	51.0	24.3	15.1	10.4	8.07	6.3	5.6	4.5	4.1	3.6	2.3	1.8	1.6	1.4
PbO@PANI-co-PTh-3	294.0	138.5	92.3	79.8	75.0	58.3	54.9	48.0	42.7	37.6	22.4	17.5	14.9	10.9

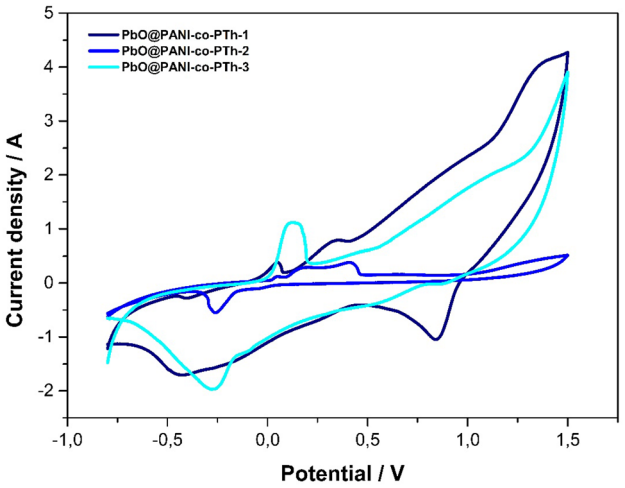

Fig. 9 Comparison of PbO@PANI-co-PTh-1, PbO@PANI-co-PTh-2 and PbO@PANI-co-PTh-3 at scanning rate of 10 mVs^{-1}

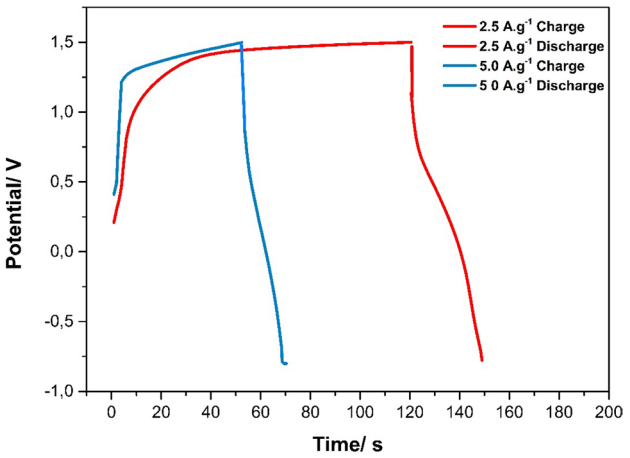

Fig. 10 GCD curves optimum PbO@PANI-co-PTh-3 asymmetric-type supercapacitors at different c

overall capacitance value. Galvanostatic performance was evaluated through various charge–discharge tests (2.5 Ag^{-1}, 5.0 Ag^{-1}), as depicted in Fig. 10. The results of the galvanostatic charge and discharge (GCD) test showed that there was almost no gap between charge and discharge curves [24, 29].

An electrochemical impedance spectroscopy (EIS) analysis was conducted to evaluate the capacitive performance of PbO@PANI-co-PTh-1, PbO@PANI-co-PTh-2, and PbO@PANI-co-PTh-3 electrodes across a frequency range spanning from 10 to 0.1 MHz, allowing for a thorough comparison of their conductivity [78, 81, 82]. EIS was performed in 1 M H_2SO_4 solution using a three-electrode setup.

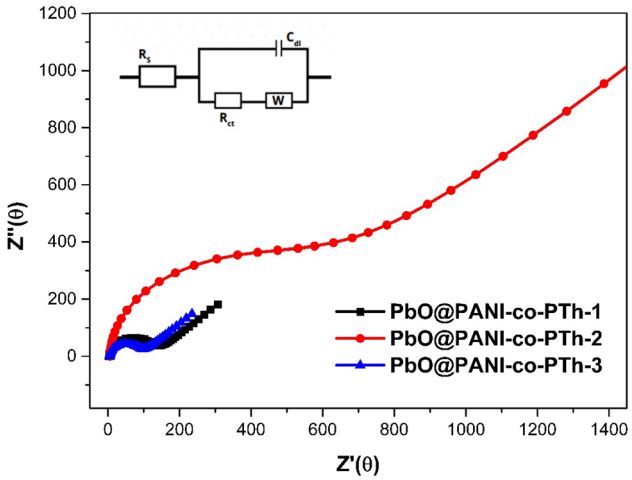

Fig. 11 Nyquist plot of supercapacitor PbO@PANI-co-PTh-1, PbO@PANI-co-PTh-2, and PbO@PANI-co-PTh-3, in 1.0 M sulfuric acid

Table 6 Fitted data for EIS test of asymmetric supercapacitor

Electrode	Rs/Ω	Cdl/F	Rct/Ω	W/ ohm $s^{-1/2}$
PbO@PANI-co-PTh-1	4.00	25.20×10^{-6}	122.8	5.503×10^{-3}
PbO@PANI-co-PTh-2	6.23	17.63×10^{-6}	531.0	609.0×10^{-6}
PbO@PANI-co-PTh-3	4.97	26.30×10^{-6}	82.3	6.730×10^{-3}

The Nyquist plots, depicted in Fig. 11, provide visual representations of the electrodes' behavior. Quantitative measurements revealed that the PbO@PANI-co-PTh-3 electrode exhibited the lowest resistance values for Rs and Rct, measuring 4.97 Ω and 82.3 Ω, respectively (Table 6). Furthermore, the incorporation of lead (II) oxide (PbO) nanoparticles within the PANI-co-PTh matrix was found to substantially increase the polymer's surface area [78]. This, in turn, led to the creation of more active regions, facilitating rapid ion movement at the electrode/electrolyte interface compared to the PbO@PANI-co-PTh-1 and PbO@PANI-co-PTh-2 materials [83]. The synergistic effects observed in the ternary composites also enhanced the binding interactions between lead(II) oxide and the PANI-co-PTh matrix, resulting in improved electrochemical performance [34, 78]. The PbO@PANI-co-PTh-3 electrode displayed not only the lowest Rs value, indicative of its highly conductive nature, but also exhibited a smaller semicircle

diameter compared to its counterparts, attributed to its smaller Rct value (Table 6). In the low-frequency range, the PbO@PANI-co-PTh-3 electrode demonstrated reduced ion diffusion resistance, facilitating rapid electrolyte ion adsorption on the electrode surface [34, 83]. This superior capacitive behavior underscores the electrode's lower ohmic and partially lower diffusion resistance, along with higher Warburg impedance, across the examined frequency range, owing to the synergistic combination of its components. Therefore, the utilization of the PbO@PANI-co-PTh-3 hybrid electrode is deemed most suitable, affirming it is as a robust material for supercapacitor applications [81, 82]. The decreasing resistance values with increasing PbO content validate the augmented distribution of PbO nanoparticles within the PANI-co-PTh matrix, expanding the polymer's surface area. Consequently, the enhancement in capacitive efficiency due to both the increased surface area and the augmentation of active regions is supported by the specific capacitance data presented in Table 4 for asymmetric-type supercapacitors [34, 78, 82, 84]. The capacitive behavior observed in cyclic voltammetry analyses was corroborated by the results of galvanostatic charge–discharge experiments. Comparing the specific capacitance value obtained for PbO@PANI-co-PTh-3 with the literature, it is evident that the specific capacitance values of the copolymer significantly increased with the addition of lead (II) oxide (Table 7). Figure 12 presents the cycling stability study of the PbO@PANI-co-PTh-3 asymmetric cell, performed across 1000 cycles within a total potential window of 2.3 V and at a scanning rate of 10 mV/s. Despite being fabricated through a straightforward process that eschews the need for high-temperature treatments, the supercapacitor device successfully preserved 70.69% of its initial capacitance after 1000 cycles. This result emphasizes the superior electrochemical stability of the asymmetrical supercapacitor, as evidenced by the consistent shape of the cyclic voltammogram even after extensive cycling. At the conclusion of the 1000 cycles, the device demonstrated a capacitance retention rate of 70.69%, confirming its robustness and durability. To further validate the stability of PbO@PANI-co-PTh-3 after 1000 cycles, SEM analysis was performed, as depicted in Fig. 13. It is noteworthy that the morphology observed after cycling reveals micro-porous yet interconnected network structures, indicating the preservation of the structure post-cyc ling.

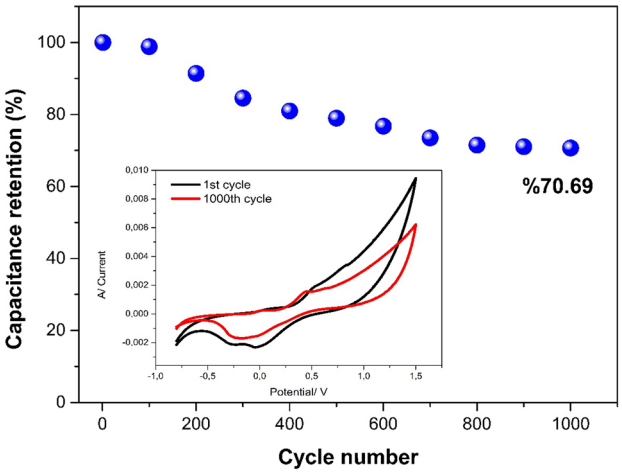

Fig. 12 Cycling performance of the PbO@PANI-co-PTh-3 asymmetric supercapacitor for 1000 cycles (inset 1st and 1000th cyclic voltammograms of the supercapacitor)

Table 7 A comparison between this study and related publications

Material	Electrolyte	Potential Range/V	Specific capacitance at charge/discharge current densities	References
Pure P3HT	0.1 M $LiClO_4$	− 0.2–1.0	160.5 Fg^{-1} at 0.5 Ag^{-1}	[63]
PEDOT-PSS:EG/rGO	1 M $LiClO_4$	0.0–1.2	174 Fg^{-1} at 0.5 Ag^{-1}	[85]
PEDOT: PSS/rGO	1 M H_2SO_4	− 0.2–0.8	249 Fg^{-1} at 0.5 Ag^{-1}	[86]
Fe_3O_4-NH-PANI	1 M H_2SO_4	− 0.5–1.0	191.2 Fg^{-1} at 0.5 $mAcm^{-2}$	[87]
PAT-AP, aniline with thiophene	1 M H_2SO_4	− 0.2–0.8	614 Fg^{-1} at 1 mVs^{-1}	[52]
PANI/rGO	1 M H_2SO_4	0.0–0.8	299 Fg^{-1} at 0.5 Ag^{-1}	[88]
PANI/TiO_2	1 M H_2SO_4	0.2–0.7	495 Fg^{-1} at 2.5 Ag^{-1}	[89]
PANI/SnO_2	1 M H_2SO_4	0.2–0.8	305 Fg^{-1} at 5 $mAcm^{-2}$	[90]
PbO@PANI-co-PTh-3	1 M H_2SO_4	− 0.8–1.5	294 Fg^{-1} at 10 mVs^{-1}	This work

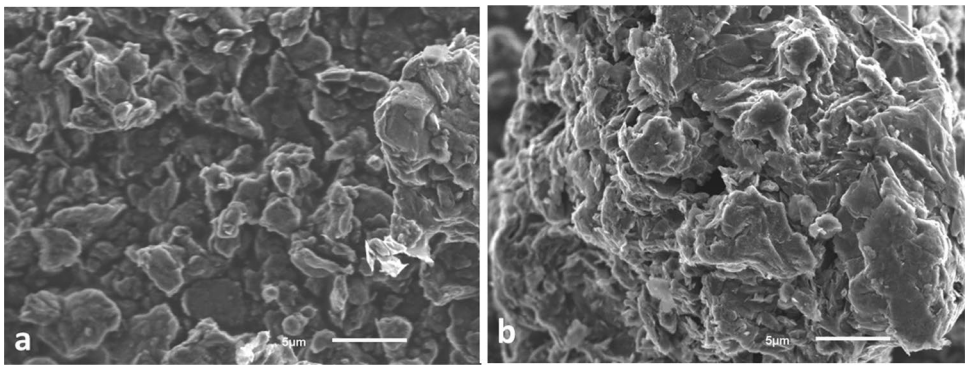

Fig. 13 SEM images of the PbO@PANI-co-PTh-3 **a** at beginning and **b** after 1000 cycle

4 Conclusion

This study significantly advances the understanding of lead (II) oxide (PbO) and PANI-co-PTh composites in asymmetric-type supercapacitor applications. Through chemical polymerization and comprehensive characterization techniques, including BET, SEM, FT-IR, and TGA, the properties of these composites were thoroughly examined. SEM following the inclusion of PbO into the PANI-co-PTh nanocomposite, revealing a uniform distribution on the nano-layers, analyzed the surface morphology. The development of the nanocomposite enhances the material's surface area and wettability due to the facile permeability of electrolyte ions in the electrode, thereby increasing its specific capacitance. The effect of PbO on PANI-co-PTh, which increases the BET surface area and facilitates superior charge transfer along the electrode–electrolyte interfaces, enhances the performance of the PbO@PANI-co-PTh-3 hybrid electrode material. The highest specific capacitance achieved was 294 Fg^{-1} in a supercapacitor prepared with PbO@PANI-co-PTh-3 and 1.0 M sulfuric acid electrolyte at a scanning rate of 10 mVs^{-1}. The results indicate a direct relationship between the surface area of CPs and their specific capacitance, with PANI-co-PTh-6 demonstrating the highest specific capacitance due to its superior surface area. Additionally, cyclic voltammetry, electrochemical impedance spectroscopy, and galvanostatic charge–discharge tests confirmed the excellent electrochemical performance of these materials in 1 M H_2SO_4 solution. PbO@PANI-co-PTh-3 retained 70.69% of its initial capacity after 1000 cycles, indicating remarkable durability. EIS studies confirm lower Rs (4.97 Ω) and Rct (82.3 Ω) values obtained for the PbO@PANI-co-PTh-3 electrode compared to other electrodes prepared, leading to improved capacitive performance. Consequently, the PbO@PANI-co-PTh-3 electrode material emerges as another contender for supercapacitor electrode materials.

Acknowledgements

Ayşe V. HACINECİPOĞLU acknowledges the support provided by TUBITAK-BIDEB and YÖK100/2000 for her PhD scholarship. M. Gencten thanks to TÜBA for Outstanding Young Scientists Awards (GEBİP). This study was supported by TUBITAK under the 2209-A University Students Research Projects Support Program with the code number 1919B012108584.

Author contributions

AH: Data analysis, Writing—original draft, Investigation, Visualization SE: Data analysis, Investigation, BK: Data analysis, Investigation, BB: Data analysis, Investigation, MG: Writing—review & editing, Methodology, Supervision, Investigation, Conceptualization.

Funding

Open access funding provided by the Scientific and Technological Research Council of Türkiye (TÜBİTAK). Funding was supported by TÜBİTAK, 1919B012108584.

Data availability

All data generated or analyzed during this study are included in this published article (and its supplementary information files).

Declarations

Conflict of interest The authors declare that they have no known competing financial interests or personal relationships that could have appeared to influence the work reported in this paper.

References

1. E. Barbera, A. Mio, A. Massi Pavan, A. Bertucco, M. Fermeglia, Energy Convers. Manag. **252**, 115072 (2022)
2. A.V. Hacınecipoğlu, M. Gençten, M.B. Arvas, Y. Sahin, ECS J. Solid State Sci. Technol. **11**, 081014 (2022)
3. A.V. Keskin, M. Gençten, S. Bozar, M.B. Arvas, S. Güneş, Y. Sahin, Thin Solid Films **706**, 138093 (2020)
4. J. Mitali, S. Dhinakaran, A.A. Mohamad, Energy Storage Sav. **1**, 166 (2022)
5. G. Abbate, E. Saraceno, A. Damasco, Supercapacitor for future energy storage. Sustain. Resour. Tomorrow (2020). https://doi.org/10.1007/978-3-030-27676-8_11
6. V. Keskin, J. Sci. Rep.-A (2023). https://doi.org/10.59313/jsr-a.1197773
7. S.H. Pour Rahmati Khalejan, V. Keskin, Tehnički Vjesnik **29**, 1889 (2022)
8. V. Keskin, A. Gupta, G. Szulczewski, Mater. Lett. **159**, 305–308 (2015)
9. N. Samartzis, K. Bhorkar, M. Athanasiou, L. Sygellou, V. Dracopoulos, T. Ioannides, S.N. Yannopoulos, Carbon N Y **201**, 941 (2023)
10. M. Gencten, Y. Sahin, Int. J. Energy Res. **44**, 7903 (2020)
11. N. Kocyigit, M. Gencten, M. Sahin, Y. Sahin, Int. J. Energy Res. **45**, 16176 (2021)
12. M. Pershaanaa, S. Bashir, S. Ramesh, K. Ramesh, J Energy Storage **50**, 104599 (2022)
13. K. Naoi, Y. Nagano, Supercapacitor: Mater. Syst. Appl. **20**, 239 (2013)
14. S. Karthikeyan, B. Narenthiran, A. Sivanantham, L.D. Bhatlu, T. Maridurai, Mater Today Proc **46**, 3984 (2021)
15. Z.S. Iro, C. Subramani, S.S. Dash, Int. J. Electrochem. Sci. **11**, 10628 (2016)
16. G. Wang, L. Zhang, J. Zhang, Chem. Soc. Rev. **41**, 797 (2012)
17. Q. Meng, K. Cai, Y. Chen, L. Chen, Nano Energy **36**, 268 (2017)
18. S. Pande, B. Pandit, S.F. Shaikh, M. Ubaidullah, Conductive polymer and composites for supercapacitor applications, in *Recent advancements in polymeric materials for electrochemical energy storage*. (Singapore Springer Nature, Singapore, 2023), pp.71–92
19. M. Zhong, M. Zhang, X. Li, Carbon Energy **4**, 950 (2022)
20. Q. Chen, X. Wang, F. Chen, N. Zhang, M. Ma, Chem. Eng. J. **368**, 933 (2019)
21. A.K. Thakur, M. Majumder, R.B. Choudhary, S.N. Pimpalkar, IOP Conf Ser Mater Sci Eng **149**, 012166 (2016)
22. S.W. Thomas, R.R. Khan, K. Puttananjegowda, W. Serrano-Garcia, *Advances in nanostructured materials and nanopatterning technologies* (Elsevier, Amsterdam, 2020), pp.243–271
23. E. Karaca, D. Gökcen, N.Ö. Pekmez, K. Pekmez, Synth. Met. **247**, 255 (2019)
24. P. Naskar, A. Maiti, P. Chakraborty, D. Kundu, B. Biswas, A. Banerjee, J. Mater. Chem. A Mater. **9**, 1970 (2021)
25. Z. Zhai, L. Zhang, T. Du, B. Ren, Y. Xu, S. Wang, J. Miao, Z. Liu, Mater. Des. **221**, 111017 (2022)
26. A. Nk, B. Ashok, P. Tamilmani, N.K. Anushkannan, R. Dhamdhere, V. Saravanan, M. Anusuya, J. East China Univ. Sci. Technol. **65**, 1006 (2022)
27. E. Dhandapani, S. Thangarasu, S. Ramesh, K. Ramesh, R. Vasudevan, N. Duraisamy, J. Energy Storage **52**, 104937 (2022)
28. K. Namsheer, C.S. Rout, RSC Adv. **11**, 5659 (2021)
29. R. Holze, *Metal oxides in supercapacitors* (Elsevier, Amsterdam, 2017), pp.219–245

30. Y. Yang, Y. Hao, J. Yuan, L. Niu, F. Xia, Carbon N Y **78**, 279 (2014)
31. S.R. Takpire, S.A. Waghuley, J. Mater. Sci. Mater. Electron. **27**, 1007 (2016)
32. H. Xu, Z. Hai, J. Diwu, Q. Zhang, L. Gao, D. Cui, J. Zang, J. Liu, C. Xue, J. Nanomater. **2015**, 1 (2015)
33. S.C. Karadeniz, V. Ugraskan, B. Isik, F. Cakar, Colloid Polym. Sci. **301**, 1209 (2023)
34. M.A. Raza, Z.U. Rehman, M.G. Tanvir, M.F. Maqsood, *Renewable polymers and polymer-metal oxide composites* (Elsevier, Amsterdam, 2022), pp.195–251
35. N.S. Shaikh, S.B. Ubale, V.J. Mane, J.S. Shaikh, V.C. Lokhande, S. Praserthdam, C.D. Lokhande, P. Kanjanaboos, J. Alloys Compd **893**, 161998 (2022)
36. L. Fu, Q. Qu, R. Holze, V.V. Kondratiev, Y. Wu, J. Mater. Chem. A Mater. **7**, 14937 (2019)
37. M.A.A. Mohd Abdah, N.H.N. Azman, S. Kulandaivalu, Y. Sulaiman, Mater. Des. **186**, 108199 (2020)
38. S.R.P. Gnanakan, M. Rajasekhar, A. Subramaniaa, Int. J. Electrochem. Sci. **4**, 1289 (2009)
39. B. Senthilkumar, P. Thenamirtham, R. Kalai Selvan, Appl. Surf. Sci. **257**, 9063 (2011)
40. S. Dey Sadhu, P.L. Meena, J. Kumar, J. Gupta, S. Choudhary, A. Gupta, Polym. Compos.. Compos. **41**, 4619 (2020)
41. U. Mehmood, A. Al-Ahmed, I.A. Hussein, Renew. Sustain. Energy Rev. **57**, 550 (2016)
42. A.R. Peringath, M.A.H. Bayan, M. Beg, A. Jain, F. Pierini, N. Gadegaard, R. Hogg, L. Manjakkal, J. Energy Storage **73**, 108811 (2023)
43. E. Piçakçi, Z.G. Yalçin, Black Sea J. Eng. Sci. **6**, 375 (2023)
44. S. Abraham, M. Agnel, M.M. Antoinette, S.P. Jose, *AIP conference proceedings* (AIP Publishing, College Park, 2021), p.020118
45. H. Sivaram, D. Selvakumar, A. Alsalme, A. Alswieleh, R. Jayavel, J. Alloys Compd. **731**, 55 (2018)
46. W. Du, X. Wang, J. Zhan, X. Sun, L. Kang, F. Jiang, X. Zhang, Q. Shao, M. Dong, H. Liu, V. Murugadoss, Z. Guo, Electrochim. Acta **296**, 907 (2019)
47. H. Jiang, Q. Mu, H. Kimura, R. Liu, W. Yang, L. Liu, W. Du, C. Hou, Prog. Nat. Sci.: Mater. Int. **33**, 743 (2023)
48. W. Yang, D. Peng, H. Kimura, X. Zhang, X. Sun, R.A. Pashameah, E. Alzahrani, B. Wang, Z. Guo, W. Du, C. Hou, Adv. Compos. Hybrid Mater. **5**, 3146 (2022)
49. S. Ahmed, A. Ahmed, D.B. Basha, S. Hussain, I. Uddin, M.A. Gondal, Synth. Met. **295**, 117326 (2023)
50. A.I. Torvi, S.R. Naik, S.N. Hegde, M. Mulla, R.R. Kamble, G.R. Mitchell, M.Y. Kariduraganavar, *Flexible supercapacitor nanoarchitectonics* (Wiley, Hoboken, 2021), pp.611–634
51. B. Ok, M. Gencten, M.B. Arvas, Y. Sahin, ECS J. Solid State Sci. Technol. **11**, 033004 (2022)
52. U. Male, B.S. Singu, P. Srinivasan, J. Appl. Polym. Sci. Polym. Sci. (2015). https://doi.org/10.1002/app.42013
53. H.J. Jang, C.-S. Park, E.Y. Jung, G.T. Bae, B.J. Shin, H.-S. Tae, Polymers (Basel) **12**, 2225 (2020)
54. K. Kaneto, K. Yoshino, Y. Inuishi, Solid State Commun. **46**, 389 (1983)
55. D. Thanasamy, D. Jesuraj, S.K. Konda Kannan, V. Avadhanam, Polymer (Guildf) **175**, 32 (2019)
56. M. Ates, A.S. Sarac, Polym. Plast. Technol. Eng. **50**, 1130 (2011)
57. R. Jamal, Y. Osman, A. Rahman, A. Ali, Y. Zhang, T. Abdiryim, Materials **7**, 3786 (2014)
58. Y.A. Udum, K. Pekmez, A. Yıldız, Eur. Polym. J. **41**, 1136 (2005)
59. B. Ok, M. Gencten, M.B. Arvas, Y. Sahin, J. Mater. Sci. Mater. Electron. **34**, 1690 (2023)
60. S. Yasa, O. Kumbasi, M.B. Arvas, M. Gencten, M. Sahin, Y. Sahin, ECS J. Solid State Sci. Technol. **12**, 051002 (2023)
61. M.B. Arvas, N. Karatepe, M. Gencten, Y. Sahin, New J. Chem. **45**, 6928 (2021)
62. M.B. Arvas, N. Karatepe, M. Gencten, Y. Sahin, Int. J. Energy Res. **46**, 7348 (2022)
63. A. Shokry, M. Karim, M. Khalil, S. Ebrahim, J. El Nady, Sci. Rep. **12**, 11278 (2022)
64. F. Li, N. Wu, H. Kimura, Y. Wang, B. Bin Xu, D. Wang, Y. Li, H. Algadi, Z. Guo, W. Du, C. Hou, Nanomicro. Lett. **15**, 220 (2023)
65. F. Li, Q. Li, H. Kimura, X. Xie, X. Zhang, N. Wu, X. Sun, B. Bin Xu, H. Algadi, R.A. Pashameah, A.K. Alanazi, E. Alzahrani, H. Li, W. Du, Z. Guo, C. Hou, J. Mater. Sci. Technol. **148**, 250 (2023)
66. D. Wu, X. Xie, Y. Ma, J. Zhang, C. Hou, X. Sun, X. Yang, Y. Zhang, H. Kimura, W. Du, Chem. Eng. J. **433**, 133673 (2022)
67. C. Hou, F. Li, H. Kimura, Q. Li, L. Liu, Q. Chu, J. Wu, G. Fan, W. Du, J. Market. Res. **25**, 5148 (2023)
68. M. Ohira, T. Sakai, M. Takeuchi, Y. Kobayashi, M. Tsuji, Synth. Met. **18**, 347 (1987)
69. S. Vinodh Kumar, S. Mukherjee, J.B.M. Krishna, D. Das, A. Saha, J. Appl. Polym. Sci.Polym. Sci. **114**, 2792 (2009)
70. S.S. Bangade, V.M. Raut, S.E. Bhandarkar, D.P. Gulwade, Mater. Today Proc. **29**, 1067 (2020)
71. Z. Karimi, R. Khalili, M. Aliza Zouli, Water Sci. Technol. **84**, 182 (2021)

72. N.S. Wadatkar, S.A. Waghuley, J. Mater. Sci. Mater. Electron. **27**, 10573 (2016)
73. C. Hou, W. Yang, H. Kimura, X. Xie, X. Zhang, X. Sun, Z. Yu, X. Yang, Y. Zhang, B. Wang, B. Bin Xu, D. Sridhar, H. Algadi, Z. Guo, W. Du, J. Mater. Sci. Technol. **142**, 185 (2023)
74. Q. Mu, R. Liu, H. Kimura, J. Li, H. Jiang, X. Zhang, Z. Yu, X. Sun, H. Algadi, Z. Guo, W. Du, C. Hou, Adv Compos Hybrid Mater **6**, 23 (2023)
75. H. Yildirimkalyon, M. Gencten, S. Gorduk, Y. Sahin, J. Energy Storage **48**, 103699 (2022)
76. O. Aydin, B. Birol, M. Gencten, Ionics (Kiel) **29**, 3335 (2023)
77. S. Yasa, O. Aydin, M. Al-Bujasim, B. Birol, M. Gencten, J. Energy Storage **73**, 109073 (2023)
78. S.P. Vinodhini, J.R. Xavier, Mater. Chem. Phys. **318**, 129233 (2024)
79. Y. He, X. Wang, P. Zhang, H. Huang, X. Li, Y. Shui, B. Chen, Z. Guo, Energy **183**, 358 (2019)
80. S. Abaci, Y. Aslan, A. Yildiz, J. Mater. Sci. **40**, 1163 (2005)
81. F. Shaheen, R. Ahmad, S. Sharif, M. Habib, R. Sharif, M. Fatima, C. Wang, Mater. Lett. **284**, 129031 (2021)
82. K.T. Kubra, A. Javaid, R. Sharif, G. Ali, F. Iqbal, A. Salman, F. Shaheen, A. Butt, F.J. Iftikhar, J. Mater. Sci. Mater. Electron. **31**, 12455 (2020)
83. R. Ganesan, J.R. Xavier, Mater. Sci. Eng. B **300**, 117101 (2024)
84. J.R. Xavier, J. Appl. Electrochem.. Appl. Electrochem. **21**, 1–22 (2024)
85. S. Khasim, A. Pasha, N. Badi, M. Lakshmi, Y.K. Mishra, RSC Adv. **10**, 10526 (2020)
86. G. Liu, X. Chen, J. Liu, C. Liu, J. Xu, Q. Jiang, Y. Jia, F. Jiang, X. Duan, P. Liu, Electrochim. Acta **365**, 137363 (2021)
87. V.S. Patil, S.S. Thoravat, S.S. Kundale, T.D. Dongale, P.S. Patil, S.A. Jadhav, Chem. Phys. Lett. **814**, 140334 (2023)
88. N. Macherla, K. Singh, M.S. Santosh, K. Kumari, R.G.R. Lekkala, Colloids Surf A Physicochem Eng AspPhysicochem. Eng. Asp **612**, 125982 (2021)
89. X. Li, H. Zhang, G. Wang, Z. Jiang, J. Mater. Chem. **20**, 10598 (2010)
90. Z.-A. Hu, Y.-L. Xie, Y.-X. Wang, L.-P. Mo, Y.-Y. Yang, Z.-Y. Zhang, Mater. Chem. Phys. **114**, 990 (2009)